*Economic Geology*, v. 108, pp. 1889–1901

# The Origin of Ni-Cu-PGE Sulfide Mineralization in the Margin of the Zhubu Mafic-Ultramafic Intrusion in the Emeishan Large Igneous Province, Southwestern China

Qingyan Tang,[1] Yansheng Ma,[2] Mingjie Zhang,[1,†] Chusi Li,[3] Dan Zhu,[2] and Yan Tao[2,†]

[1] *School of Earth Sciences and Gansu Key Laboratory of Mineral Resources in Western China, Lanzhou University, Lanzhou 730000, China*

[2] *State Key Laboratory of Ore Deposit Geochemistry, Institute of Geochemistry, Chinese Academy of Science, Guiyang 550002, China*

[3] *Department of Geological Sciences, Indiana University, Bloomington, Indiana 47405*

## Abstract

The Zhubu magmatic Ni-Cu-PGE sulfide deposit is hosted in a mafic-ultramafic intrusion which is part of the Emeishan large igneous province in southwest China. The Zhubu intrusion is composed of a layered sequence (750 × 400 × 600 m) with subhorizontal modal layering and a subvertical marginal zone of <40 m across. The marginal zone is composed of lherzolite and olivine websterite with minor gabbroic rocks. The layered sequence is composed of lherzolite, websterite, gabbro, and gabbrodiorite from the base to the top. The Zhubu intrusion can be explained by two stages of formation, an early conduit stage for the marginal zone and a late in situ differentiation stage for the layered sequence. Most important Ni-Cu-PGE mineralization in the intrusion occurs as disseminated sulfides within the marginal zone. Olivine crystals from the marginal zone contain 81 to 84 mol % Fo and 1,600 to 1,900 ppm Ni. The rims of zoned olivine phenocrysts in the Emeishan picrites have similar Fo contents but significantly higher Ni contents (2,300–2,600 ppm). The olivine data indicate that the parental magma of the Zhubu ultramafic rocks is similar to the transporting magma of the Emeishan picrites in MgO/FeO ratios but depleted in Ni due to sulfide segregation before olivine crystallization. The initial concentrations of PGE in the Zhubu magma, estimated from bulk sulfide compositions, are 7 ppb Pd, 9.3 ppb Pt, and 0.8 ppb Ir, similar to the values in the Emeishan picrites. Like the Emeishan picrites, the Zhubu intrusive rocks are characterized by light REE enrichments. Negative Nb anomalies relative to Th and Ta, which are rare in the Emeishan picrites, are present in the Zhubu samples. The $(^{87}Sr/^{86}Sr)_i$ and $\varepsilon_{Nd}$ values of the Zhubu intrusive rocks vary from 0.709591 to 0.710692 and from –2 to –3, respectively. The trace element and isotope compositions indicate that the Zhubu magma was contaminated by crustal materials, supporting the interpretation that sulfide saturation in the magma was triggered by crustal contamination. The area where the lower part of the conduit may have been brought up by faulting should be the focus of future exploration at Zhubu.

## Introduction

Mafic-ultramafic intrusions associated with continental flood basalts are important hosts to magmatic sulfide deposits (see summary in Naldrett, 2011). The best examples are the Noril'sk-Talnakh Ni-Cu-PGE deposits that formed in the plumbing systems of the Siberian flood basalts (Lightfoot and Keays, 2005; Li et al., 2009; Arndt, 2011). The Emeishan flood basalts erupted at ~260 Ma (Fan et al., 2008), ~9 Ma before the Siberian flood basalts (~251 Ma: Kamo et al., 2003). The Permian flood basalts, picrites and associated mafic-ultramafic intrusions in the Emeishan region, southwest China (Fig. 1) are collectively referred to as the Emeishan large igneous province in the literature. Recent studies reveal that some contaminated basalts in the Emeishan large igneous province are depleted in PGE (Qi and Zhou, 2008; Song et al., 2009; Wang et al., 2011), whereas the associated picrites are not (Wang et al., 2007; Li et al., 2012). This indicates that sulfide saturation as the result of crustal contamination took place in some parts of the plumbing systems of the Emeishan large igneous province, which in turn indicates that some of the subvolcanic intrusions may host important magmatic Ni-Cu-PGE sulfide deposits. Recently, several magmatic Ni-Cu-PGE sulfide deposits in the Emeishan large igneous province have been investigated for their origins. These include the Baimazhai, Limahe and Nantianwan Ni-Cu deposits (Wang et al., 2006, 2012; Tao et al., 2008, 2010), the Yangliuping Ni-Cu-(PGE) deposit (Song et al., 2003), and the Jinbaoshan PGE deposit (Wang et al., 2005; Tao et al., 2007). The Zhubu Ni-Cu-PGE deposit in the Emeishan large igneous province was discovered a half century ago (TGT-YBGR, 1970) but no study has been reported in international journals. In this paper we present the results of an integrated mineralogical and geochemical study of the Zhubu deposit.

†Corresponding authors: e-mail: mjzhang@lzu.edu.cn; taoyan@vip.gyig.ac.cn

## Geology of the Zhubu Deposit

The Zhubu intrusion is located in the central part of the Emeishan large igneous province (Fig. 1). The SHRIMP U-Pb age of zircons from the intrusion is 261 ± 2 Ma (Zhou et al., 2008). Its surface exposure is ~750 m long and ~400 m wide (Fig. 2a). The downward extension of the intrusion exceeds 580 m (Fig. 2b). The Zhubu intrusion is composed of a layered sequence and a marginal zone wrapping around the layered sequence. The layered sequence represents >90 vol % of the intrusion and is characterized by subhorizontal modal layering. Ultramafic rocks such as lherzolite and olivine websterite occur at the bottom; mafic rocks such as gabbro and gabbrodiorite occur at the top (Fig. 2b). The contacts between the different rock units in the entire layered sequence are gradational. The marginal zone is discordant with the layered

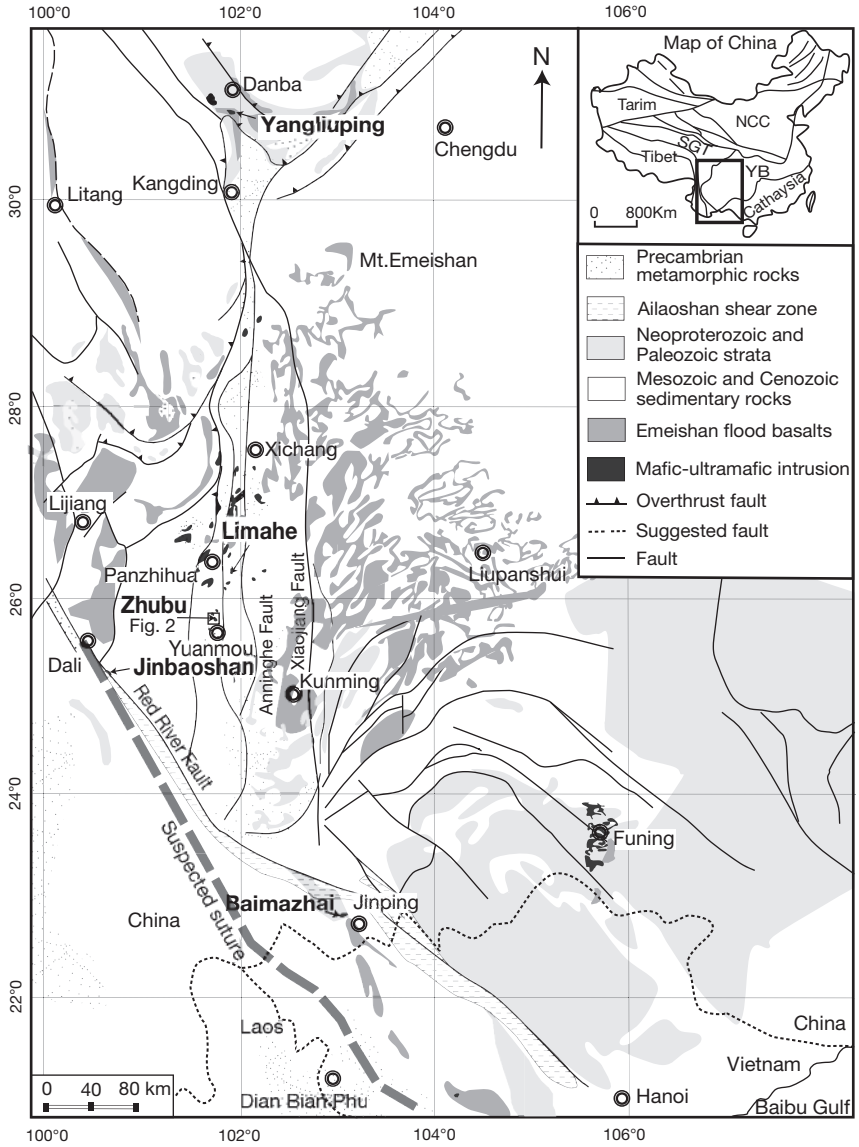


FIG. 1. Distribution of Emeishan flood basalts and associated mafic-ultramafic intrusions (modified from Chung and Jahn, 1995; Song et al., 2001; Li et al., 2012). NCC = north China craton, SGT = Songpan-Ganzi terrane.

sequence (Fig. 2b). No chilled rocks are present between the marginal zone and the layered sequence. A hornfels zone of 0.5 to 1 m in thickness is present between the marginal zone and Precambrian gneissic country rocks. The marginal zone is ~10 to 40 m across. It is composed of lherzolite, olivine websterite, websterite, and contaminated gabbroic rocks. Small gneissic inclusions (<10 cm diam) are present in places in the gabbroic rocks.

Most important sulfide mineralization in the Zhubu intrusion occurs mainly as disseminated sulfides (pyrrhotite, pentlandite, and chalcopyrite) within the marginal zone. Small lenses of disseminated sulfides are also present within the layered sequence, but they are volumetrically insignificance. Nickel and Cu grades are up to 0.8 wt %; Pt and Pd grades are up to 3 ppm (Fig. 2c). Drilling results show that metal variations across the marginal zone are irregular (TGT-YBGR, 1970). The total resources of the deposit have never been reported to the public. The deposit was mined by small open pits several years ago when the prices of Ni and Pt were high.

## Samples and Petrography

The samples used in this study were collected from outcrops and the walls of an open pit in the western part of the intrusion. Sample locations are shown in Figure 2a. Twelve samples from the marginal zone in the western part of the intrusion are lherzolite and olivine websterite. Three samples from the marginal zone in the northern part of the intrusion are lherzolite, gabbro and gabbrodiorite. Ten samples from the layered sequence are olivine websterite, gabbro, and gabbrodiorite.

Lherzolite contains 40 to 60% (modal) olivine, 30 to 40% pyroxenes (clinopyroxene and orthopyroxene approximately in equal proportion), plus minor hornblende and phlogopite (Fig. 3a, b). Small chromite crystals and sulfide inclusions

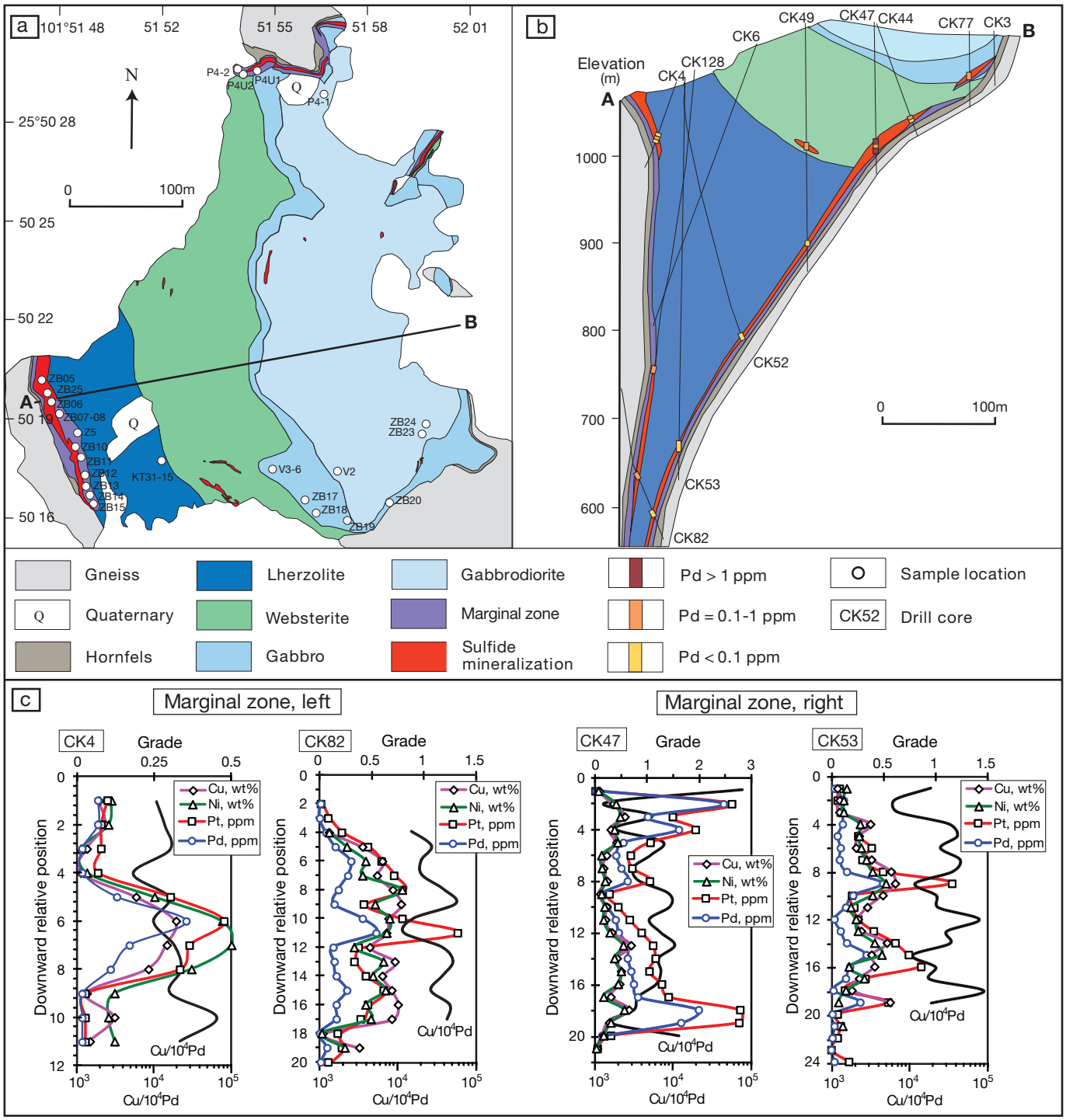


FIG. 2. Simplified geologic map (a), cross section (b), and metal variations across the marginal zone (c) of the Zhubu mafic-ultramafic intrusion (modified from TGT-YBGR, 1970).

within olivine crystals are present in some samples. Olivine is a cumulus phase (Fig. 3a) and pyroxenes, hornblende and phlogopite occur in the interstitial spaces (Fig. 3b). Olivine websterite contains 20 to 30% olivine, 50 to 60% pyroxenes, and minor amounts of plagioclase, hornblende, and phlogopite. Olivine crystals in this rock are commonly enclosed in large orthopyroxene crystals (Fig. 3c). Websterite contains about 95% pyroxenes with minor amounts of olivine and plagioclase. Orthopyroxene commonly occurs as large crystals enclosing small olivine crystals. Clinopyroxene, plagioclase, hornblende, and phlogopite occur in the interstitial spaces. Gabbro contains <5% olivine, 40 to 45% pyroxenes, 40 to 50% plagioclase, and minor hornblende and phlogopite. Gabbrodiorite contains 30 to 40% plagioclase, 15 to 25% clinopyroxene,

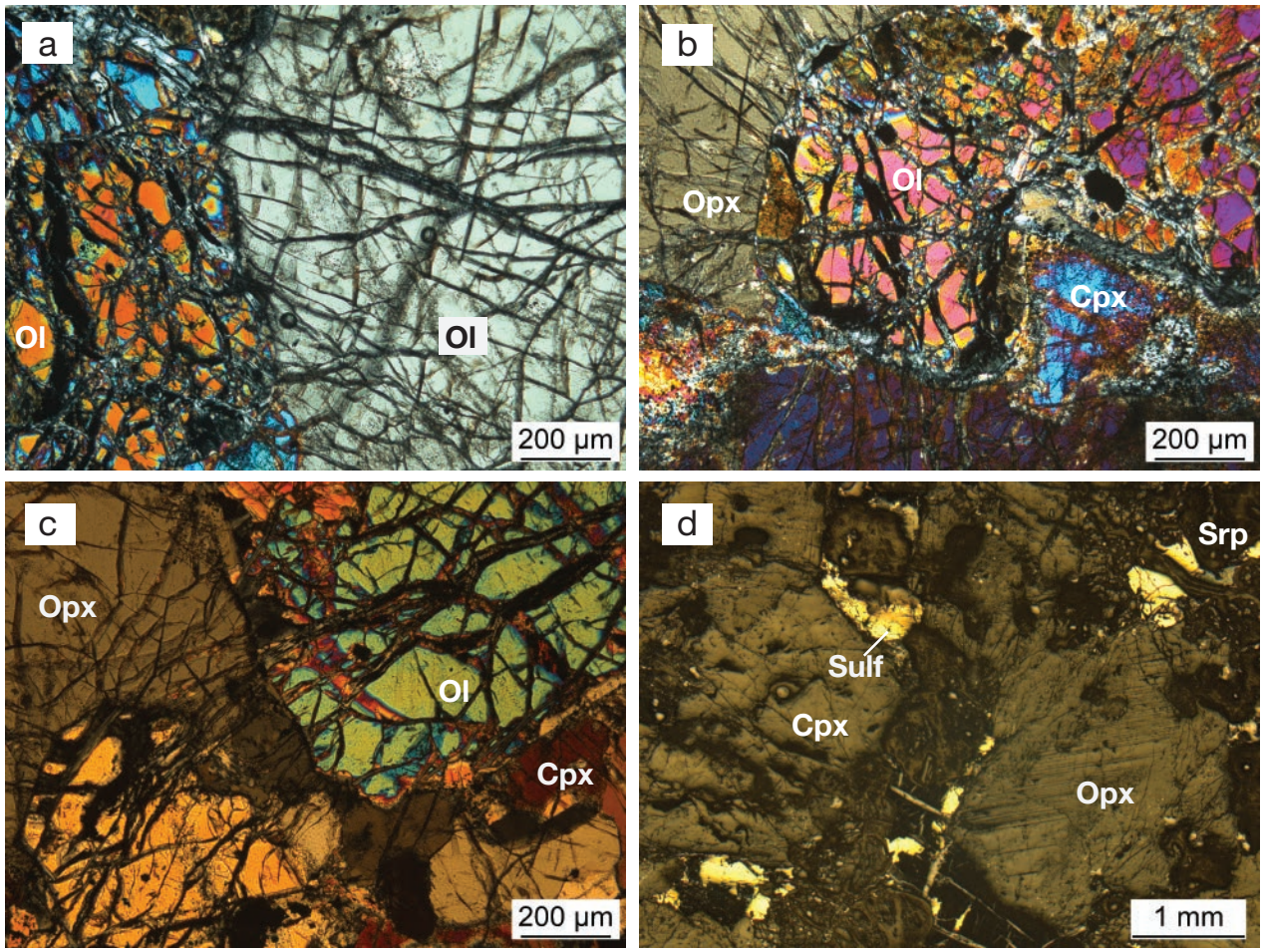


FIG. 3. Photomicrographs of representative rock samples from the Zhubu intrusion. (a) and (b) lherzolite, (c) olivine websterite, (d) sulfide-mineralized olivine websterite. Abbreviations: Cpx = clinopyroxene, Ol = olivine, Opx = orthopyroxene, Srp = serpentine, Sulf = sulfides.

20 to 30% hornblende, 5 to 10% biotite, and 10 to 15% Fe-Ti oxides.

Partial alterations of olivine by serpentine + magnetite, orthopyroxene by talc, clinopyroxene by secondary amphibole (actinolite or tremolite) or chlorite, and plagioclase by sericite + epidote + albite are present in the samples. Disseminated sulfides are partially replaced by secondary magnetite in some samples (Fig. 3d).

## Analytical Methods

Mineral compositions were determined by wavelength dispersive X-ray analysis using a CAMECA SX50 electron microprobe at Indiana University. The analytical conditions for major elements were 15 kV, 20-nA beam current, 1-$\mu$m beam size, and peak-counting time of 20 s. Nickel in olivine was analyzed using a beam current of 100 nA and a peak-counting time of 50 s. The detection limit for Ni under such conditions is ~100 ppm. International mineral standards such as San Carlos olivine (USNM 1113122) were used for calibration. Analytical reproducibility was within 2% relative.

Major and trace element concentrations in whole rocks were analyzed by XRF and ICP-MS, respectively, in the State Key Laboratory of Ore Deposit Geochemistry, Institute of Geochemistry, Chinese Academy of Sciences. Rock powders were fused to form glass disks. The glass disks were then analyzed by XRF using a Rigaku ZSX100e instrument. The solutions of acid-digested rock powders in steel-jacketed Teflon "bombs" were analyzed by ICP-MS using a Perkin-Elmer Sciex ELAN 6000 instrument. The analytical precisions for major elements and most trace elements were better than 5% relative.

Whole-rock PGE abundances were determined using the method of Qi et al. (2011) in the State Key Laboratory of Ore Deposit Geochemistry, Institute of Geochemistry, Chinese Academy of Sciences. Ten grams of sample powders were dissolved by HF in customized 120-ml PTFE beakers on a hot plate. The dried residues were then digested by HF + $HNO_3$ in stainless steel pressure bombs at 190°C for ~48 h. The solutions were analyzed using an ELAN DRC-e ICP-MS instrument. The detection limits are <0.02 ppb for Pt and Pd, and <0.01 ppb for Ir, Ru, and Rh (Qi et al., 2011).

Whole-rock Rb-Sr and Sm-Nd isotopes were determined using a Finnigan MAT 262 thermal ionization mass spectrometer in the Institute of Geology and Geophysics, Chinese Academy of Science in Beijing. The powders were treated with 0.3 *N* HCl for 1 h at ~100°C, and dried after rinsing with

purified water. The samples were weighed and spiked with mixed isotope tracers, and then dissolved in Teflon capsules with HF + $HNO_3$ at 120°C for 7 days. Procedural blanks were <100 pg for Sm and Nd, and <500 pg for Rb and Sr. Mass fractionation corrections for Sr and Nd isotope ratios were based on values of $^{86}Sr/^{88}Sr$ = 0.1194 and $^{146}Nd/^{144}Nd$ = 0.7219. The precision ($2\sigma$) for Sr and Nd isotope ratios is less than 1% relative. The measured values for the La Jolla Nd standard and the NBS-987 Sr standard were $^{143}Nd/^{144}Nd$, 0.511849 ± 10 and $^{87}Sr/^{86}Sr$, 0.710221 ± 13, respectively.

## Results

### *Mineral chemistry*

Representative analyses of olivine, clinopyroxene, and chromite from the Zhubu intrusion are given in the Appendix (Table A1). A comparison of olivine compositions in samples containing no visible sulfides from three sulfide ore-bearing mafic-ultramafic intrusions (Zhubu, Limahe, and Jinbaoshan) is illustrated in Figure 4. The Fo and Ni contents of olivine from the ultramafic intrusive rocks are similar, varying between 81 and 84 mol %, and between 1,600 and 1,900 ppm, respectively. The Ni contents of olivine from the ultramafic intrusive rocks are ~500 ppm lower than that of olivine with similar Fo contents from the Emeishan picrites (Fig. 4).

Cr spinel inclusions within olivine crystals in the Zhubu intrusion contain ~8 wt % $Al_2O_3$ and ~36 wt % $Cr_2O_3$ and have a Cr number (100 × Cr/(Cr + Al), molar) of ~75. These values are slightly lower than that of the Emeishan picrites but are similar to that of the Limahe sulfide ore-bearing intrusion (Li et al., 2008). Clinopyroxene crystals in the Zhubu ultramafic rocks have lower Mg numbers (100 × Mg/(Mg + $Fe^{total}$), molar), higher $Cr_2O_3$ and lower $TiO_2$ contents than clinopyroxene phenocrysts in the Emeishan picrites (Fig. 5).

### *Major and trace elements*

Whole-rock chemical compositions of the Zhubu intrusion are given in Table 1. In order to compare the compositions of constituent minerals directly, we have normalized the original

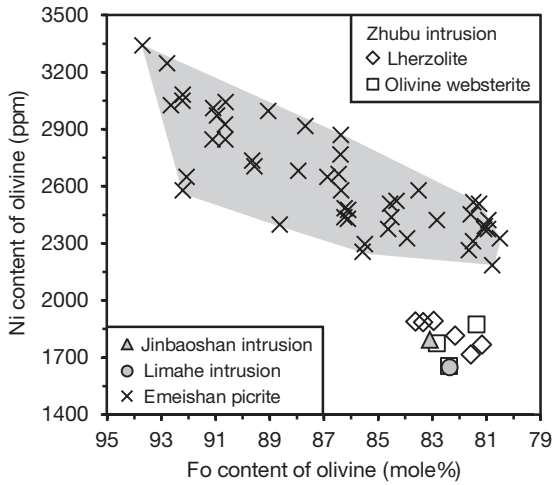


FIG. 4. Plot of Ni vs. Fo contents in olivine. Data for the Zhubu intrusion are from this study (Table A1). Data for Limahe intrusion are from Tao et al. (2008). Data for the Jinbaoshan intrusion are from Tao et al. (2007). Data for the Emeishan picrites are from Li et al. (2012).

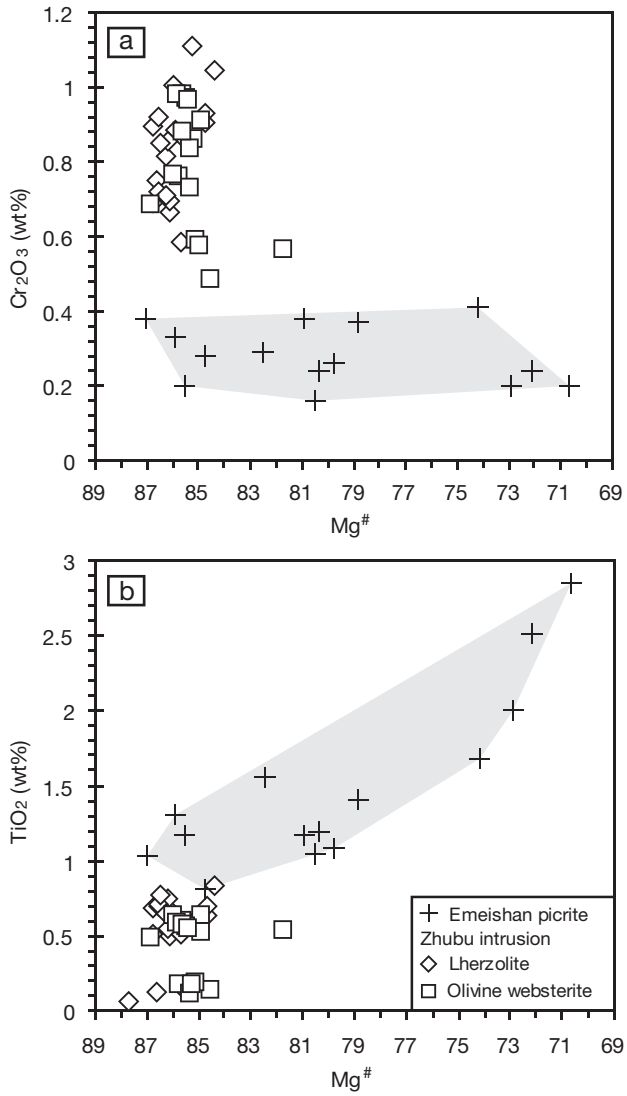


FIG. 5. Plots of Mg number (100Mg/(Mg + $Fe^{total}$), molar) vs. $Cr_2O_3$ (a) and $TiO_2$ (b) of clinopyroxene. Data for the Zhubu intrusion are from this study (Table A1). Data for the Emeishan picrites are from Zhang et al. (2006).

data to 100% anhydrous silicate compositions by correcting for loss-on-ignition and base metal sulfides. The amounts of sulfides (pyrrhotite + pentlandite + chalcopyrite) in the samples were calculated using whole-rock S and Cu contents and the amounts of Ni corrected for the contribution from silicate minerals (mostly olivine) in the samples using the procedures described in Li et al. (2001). The average contents of Ni in the samples without visible sulfides were used as the correction values. As shown in Figure 6, the compositions of ultramafic rocks in the Zhubu intrusion are mainly controlled by olivine and pyroxenes; the compositions of gabbros are mainly controlled by pyroxenes and plagioclase, and the compositions of gabbrodiorites are mainly controlled by plagioclase and clinopyroxene plus significant amounts of low Si and low Ca minerals such as hornblende, biotite, and Fe-Ti oxides.

The chondrite-normalized REE and primitive mantle-normalized immobile trace element patterns of the Zhubu intrusion are illustrated in Figure 7. The trace element abundances

TABLE 1. Whole-Rock Major and Trace Element Concentrations in the Zhubu Intrusion

| Rock | Lherzolite | | | | | | | | Ol websterite | | | |
|---|---|---|---|---|---|---|---|---|---|---|---|---|
| Sample | ZB07 | ZB08 | ZB10 | ZB11 | ZB14 | ZB25 | P4-2 | Z5 | ZB05 | ZB06 | ZB12 | KT31-15 |
| $SiO_2$ | 40.62 | 40.99 | 44.42 | 44.80 | 44.27 | 39.23 | 39.25 | 39.36 | 45.28 | 46.26 | 43.87 | 45.73 |
| $TiO_2$ | 0.62 | 1.27 | 0.65 | 0.64 | 0.64 | 1.10 | 0.99 | 1.25 | 0.80 | 0.77 | 1.00 | 0.81 |
| $Al_2O_3$ | 1.99 | 2.82 | 2.03 | 1.59 | 1.68 | 3.04 | 3.31 | 2.45 | 1.96 | 1.95 | 8.53 | 2.23 |
| $FeO^{total}$ | 13.58 | 14.82 | 11.47 | 10.25 | 10.46 | 14.82 | 12.83 | 12.61 | 14.56 | 12.03 | 11.53 | 9.83 |
| MnO | 0.13 | 0.17 | 0.13 | 0.13 | 0.13 | 0.19 | 0.09 | 0.15 | 0.14 | 0.14 | 0.16 | 0.13 |
| MgO | 28.78 | 26.96 | 26.05 | 26.65 | 26.89 | 30.15 | 28.48 | 30.05 | 23.14 | 24.47 | 20.35 | 23.30 |
| CaO | 6.40 | 5.51 | 9.53 | 10.49 | 8.93 | 4.22 | 3.10 | 4.16 | 8.52 | 10.37 | 8.94 | 10.53 |
| $Na_2O$ | 0.16 | 0.13 | 0.20 | 0.18 | 0.19 | 0.11 | 0.21 | 0.38 | 0.13 | 0.19 | 0.86 | 0.38 |
| $K_2O$ | 0.09 | 0.11 | 0.06 | 0.05 | 0.08 | 0.04 | 0.11 | 0.33 | 0.05 | 0.07 | 0.54 | 0.07 |
| $P_2O_5$ | 0.06 | 0.04 | 0.04 | 0.03 | 0.04 | 0.09 | 0.10 | 0.07 | 0.03 | 0.05 | 0.13 | 0.05 |
| $Cr_2O_3$ | 0.58 | 1.19 | 0.56 | 0.57 | 0.53 | 0.69 | 0.44 | 0.53 | 0.56 | 0.52 | 0.47 | 0.47 |
| LOI | 7.21 | 6.10 | 4.64 | 4.51 | 6.06 | 6.46 | 8.85 | 6.31 | 4.50 | 2.88 | 4.02 | 5.17 |
| Total | 100.2 | 100.1 | 99.8 | 99.9 | 99.9 | 100.1 | 97.8 | 97.7 | 99.7 | 99.7 | 100.4 | 98.7 |
| Sc | 19.71 | 23.52 | 32.78 | 30.66 | 30.47 | 12.87 | 13.90 | 20.94 | 34.22 | 34.43 | 31.79 | 30.73 |
| V | 123 | 194 | 112 | 103 | 113 | 125 | 119 | 130 | 147 | 130 | 105 | 118 |
| Co | 113 | 106 | 83 | 84 | 99 | 124 | 130 | 123 | 151 | 85 | 80 | 76 |
| Rb | 3.13 | 4.88 | 1.78 | 1.38 | 2.69 | 2.12 | 7.70 | 11.20 | 2.35 | 2.25 | 1.43 | 2.48 |
| Sr | 79 | 42 | 53 | 50 | 58 | 49 | 14 | 79 | 30 | 34 | 36 | 64 |
| Y | 6.67 | 7.58 | 7.08 | 5.51 | 6.63 | 8.39 | 8.88 | 6.35 | 8.62 | 7.17 | 6.63 | 7.40 |
| Zr | 49 | 81 | 37 | 28 | 38 | 83 | 90 | 64 | 55 | 45 | 40 | 38 |
| Nb | 4.27 | 6.88 | 3.83 | 2.54 | 3.24 | 8.71 | 9.63 | 7.50 | 3.85 | 3.59 | 3.36 | 3.93 |
| Ba | 275 | 137 | 170 | 125 | 216 | 21 | 74 | 96 | 38 | 35 | 23 | 168 |
| La | 5.25 | 4.63 | 3.62 | 2.92 | 4.53 | 10.77 | 9.87 | 7.45 | 2.60 | 2.85 | 3.18 | 3.83 |
| Ce | 13.33 | 13.03 | 10.61 | 8.73 | 12.45 | 26.26 | 22.50 | 18.90 | 8.39 | 8.95 | 9.66 | 11.90 |
| Pr | 2.04 | 2.18 | 1.84 | 1.60 | 2.00 | 3.44 | 3.12 | 2.53 | 1.64 | 1.53 | 1.77 | 1.89 |
| Nd | 8.96 | 9.97 | 8.97 | 7.54 | 9.07 | 14.24 | 13.30 | 11.60 | 8.68 | 7.89 | 8.51 | 9.42 |
| Sm | 2.08 | 2.43 | 2.23 | 1.88 | 2.13 | 2.93 | 3.18 | 2.44 | 2.36 | 2.16 | 2.17 | 2.35 |
| Eu | 0.56 | 0.66 | 0.57 | 0.56 | 0.63 | 0.73 | 0.44 | 0.87 | 0.61 | 0.51 | 0.57 | 0.58 |
| Gd | 1.87 | 2.10 | 2.03 | 1.67 | 1.96 | 2.62 | 3.05 | 2.27 | 2.21 | 2.02 | 1.95 | 2.50 |
| Tb | 0.27 | 0.33 | 0.29 | 0.24 | 0.27 | 0.36 | 0.38 | 0.27 | 0.33 | 0.29 | 0.28 | 0.32 |
| Dy | 1.41 | 1.76 | 1.50 | 1.28 | 1.44 | 1.80 | 2.03 | 1.41 | 1.79 | 1.59 | 1.46 | 1.65 |
| Ho | 0.26 | 0.32 | 0.28 | 0.23 | 0.26 | 0.34 | 0.32 | 0.25 | 0.35 | 0.28 | 0.27 | 0.30 |
| Er | 0.64 | 0.82 | 0.69 | 0.59 | 0.66 | 0.88 | 0.92 | 0.59 | 0.83 | 0.70 | 0.67 | 0.74 |
| Tm | 0.09 | 0.11 | 0.10 | 0.07 | 0.09 | 0.12 | 0.10 | 0.09 | 0.11 | 0.09 | 0.09 | 0.09 |
| Yb | 0.51 | 0.65 | 0.55 | 0.44 | 0.54 | 0.70 | 0.86 | 0.54 | 0.67 | 0.54 | 0.51 | 0.57 |
| Lu | 0.07 | 0.09 | 0.08 | 0.07 | 0.08 | 0.11 | 0.10 | 0.06 | 0.10 | 0.08 | 0.07 | 0.07 |
| Hf | 1.19 | 1.91 | 1.00 | 0.86 | 1.02 | 2.05 | 2.37 | 1.73 | 1.43 | 1.20 | 1.05 | 1.14 |
| Ta | 0.31 | 0.51 | 0.27 | 0.18 | 0.24 | 0.66 | 0.63 | 0.54 | 0.28 | 0.26 | 0.24 | 0.29 |
| Th | 1.00 | 1.64 | 0.80 | 0.55 | 0.73 | 2.03 | 2.06 | 1.31 | 1.11 | 0.83 | 0.76 | 0.86 |
| U | 0.20 | 0.38 | 0.18 | 0.12 | 0.19 | 0.48 | 0.53 | 0.27 | 0.26 | 0.19 | 0.16 | 0.23 |

| Rock | Ol websterite | | Gabbro | | | | | | Gabbrodiorite | | | | |
|---|---|---|---|---|---|---|---|---|---|---|---|---|---|
| Sample | ZB13 | ZB15 | ZB17 | ZB18 | ZB19 | ZB20 | P4U2 | V3-6 | ZB23 | ZB24 | V2 | P4-1 | P4U1 |
| $SiO_2$ | 46.04 | 46.92 | 50.50 | 50.03 | 50.01 | 49.66 | 49.41 | 50.21 | 43.14 | 43.61 | 45.86 | 42.67 | 42.86 |
| $TiO_2$ | 0.70 | 0.69 | 1.83 | 2.45 | 3.55 | 2.82 | 2.33 | 1.92 | 6.16 | 4.84 | 3.83 | 5.62 | 5.97 |
| $Al_2O_3$ | 1.80 | 1.70 | 5.22 | 6.16 | 7.31 | 8.38 | 6.59 | 7.05 | 8.88 | 8.85 | 14.22 | 13.78 | 9.64 |
| $FeO^{total}$ | 9.35 | 9.77 | 9.31 | 11.25 | 10.73 | 12.70 | 10.24 | 8.60 | 20.13 | 18.67 | 13.89 | 20.50 | 18.13 |
| MnO | 0.14 | 0.13 | 0.18 | 0.17 | 0.16 | 0.18 | 0.17 | 0.16 | 0.21 | 0.17 | 0.18 | 0.20 | 0.23 |
| MgO | 24.58 | 24.52 | 15.38 | 13.57 | 11.93 | 10.63 | 13.52 | 13.31 | 7.02 | 6.65 | 5.05 | 5.84 | 7.27 |
| CaO | 11.90 | 12.03 | 14.51 | 13.24 | 12.60 | 11.58 | 12.80 | 12.60 | 8.65 | 10.13 | 9.98 | 3.97 | 8.66 |
| $Na_2O$ | 0.18 | 0.17 | 0.66 | 0.78 | 1.38 | 1.23 | 1.14 | 1.58 | 1.50 | 1.55 | 2.23 | 1.58 | 1.68 |
| $K_2O$ | 0.11 | 0.04 | 0.87 | 1.02 | 1.03 | 1.34 | 0.78 | 0.51 | 1.92 | 1.78 | 1.37 | 1.11 | 1.57 |
| $P_2O_5$ | 0.04 | 0.03 | 0.12 | 0.15 | 0.19 | 0.17 | 0.15 | 0.15 | 0.22 | 0.20 | 0.25 | 0.50 | 0.23 |
| $Cr_2O_3$ | 0.58 | 0.53 | 0.17 | 0.10 | 0.06 | 0.03 | 0.19 | 0.17 | 0.00 | 0.00 | 0.00 | 0.00 | 0.44 |
| LOI | 4.32 | 3.26 | 1.13 | 0.93 | 0.85 | 1.05 | 2.98 | 2.81 | 1.96 | 3.36 | 1.85 | 1.73 | 1.92 |
| Total | 99.7 | 99.8 | 99.9 | 99.8 | 99.8 | 99.8 | 100.3 | 99.1 | 99.8 | 99.8 | 98.7 | 97.5 | 98.6 |
| Sc | 35.34 | 34.99 | 51.56 | 47.42 | 48.72 | 49.18 | 41.35 | 47.58 | 41.30 | 37.32 | 30.40 | 37.06 | 6.79 |
| V | 121 | 112 | 243 | 278 | 310 | 386 | 264 | 242 | 738 | 691 | 525 | 681 | 79 |
| Co | 85 | 70 | 57 | 60 | 54 | 59 | 60 | 51 | 73 | 66 | 47 | 58 | 139 |
| Rb | 4.60 | 1.46 | 34.83 | 33.68 | 24.06 | 55.78 | 31.80 | 18.50 | 76.51 | 47.80 | 61.80 | 67.40 | 8.94 |
| Sr | 78 | 54 | 289 | 287 | 303 | 360 | 254 | 342 | 328 | 386 | 699 | 329 | 15 |
| Y | 6.76 | 6.38 | 20.29 | 21.57 | 22.90 | 26.36 | 20.00 | 21.00 | 26.92 | 27.14 | 25.70 | 24.80 | 6.60 |
| Zr | 40 | 30 | 138 | 189 | 216 | 218 | 166 | 161 | 262 | 267 | 236 | 101 | 57 |
| Nb | 3.29 | 2.42 | 13.65 | 17.97 | 22.32 | 22.66 | 16.90 | 17.90 | 28.37 | 25.46 | 25.80 | 33.90 | 8.69 |
| Ba | 300 | 227 | 272 | 269 | 346 | 368 | 245 | 289 | 446 | 462 | 376 | 417 | 36 |

TABLE 1. *(Cont'd.)*

| Rock | Ol websterite | | Gabbro | | | | | | Gabbrodiorite | | | | |
|---|---|---|---|---|---|---|---|---|---|---|---|---|---|
| Sample | ZB13 | ZB15 | ZB17 | ZB18 | ZB19 | ZB20 | P4U2 | V3-6 | ZB23 | ZB24 | V2 | P4-1 | P4U1 |
| La | 3.79 | 2.09 | 18.07 | 24.87 | 29.07 | 30.75 | 22.40 | 26.20 | 34.43 | 33.31 | 33.10 | 29.70 | 14.50 |
| Ce | 11.20 | 7.08 | 45.25 | 59.36 | 67.55 | 71.64 | 51.40 | 59.00 | 76.64 | 77.90 | 77.60 | 71.60 | 29.70 |
| Pr | 1.83 | 1.34 | 6.41 | 8.05 | 9.22 | 9.69 | 6.94 | 7.98 | 10.44 | 10.45 | 10.00 | 9.40 | 3.81 |
| Nd | 8.71 | 7.04 | 27.52 | 33.77 | 38.93 | 41.19 | 30.00 | 34.90 | 42.65 | 43.31 | 44.80 | 41.40 | 14.90 |
| Sm | 2.24 | 1.96 | 6.31 | 7.40 | 8.15 | 8.92 | 6.47 | 7.25 | 9.01 | 9.04 | 9.45 | 8.57 | 2.96 |
| Eu | 0.65 | 0.58 | 1.87 | 2.03 | 2.30 | 2.47 | 1.92 | 2.19 | 2.55 | 2.43 | 2.72 | 2.54 | 0.41 |
| Gd | 1.97 | 1.87 | 5.79 | 6.45 | 7.02 | 7.69 | 6.28 | 7.00 | 8.07 | 7.90 | 8.77 | 8.02 | 2.64 |
| Tb | 0.29 | 0.26 | 0.83 | 0.88 | 0.98 | 1.11 | 0.85 | 0.96 | 1.08 | 1.08 | 1.10 | 1.08 | 0.30 |
| Dy | 1.56 | 1.46 | 4.37 | 4.69 | 5.15 | 5.82 | 4.30 | 5.10 | 5.76 | 5.73 | 5.84 | 5.55 | 1.49 |
| Ho | 0.28 | 0.28 | 0.83 | 0.86 | 0.93 | 1.08 | 0.80 | 0.89 | 1.04 | 1.04 | 1.08 | 1.02 | 0.27 |
| Er | 0.66 | 0.66 | 2.05 | 2.24 | 2.33 | 2.74 | 2.05 | 2.25 | 2.66 | 2.63 | 2.69 | 2.55 | 0.71 |
| Tm | 0.10 | 0.09 | 0.29 | 0.29 | 0.30 | 0.36 | 0.26 | 0.29 | 0.35 | 0.35 | 0.33 | 0.31 | 0.09 |
| Yb | 0.55 | 0.48 | 1.63 | 1.72 | 1.81 | 2.17 | 1.58 | 1.78 | 2.04 | 2.10 | 2.09 | 1.91 | 0.51 |
| Lu | 0.08 | 0.07 | 0.23 | 0.25 | 0.26 | 0.30 | 0.23 | 0.24 | 0.30 | 0.30 | 0.27 | 0.25 | 0.07 |
| Hf | 1.05 | 0.87 | 3.64 | 5.04 | 5.42 | 5.71 | 4.76 | 4.53 | 6.64 | 6.86 | 6.47 | 3.62 | 1.43 |
| Ta | 0.23 | 0.17 | 1.06 | 1.32 | 1.75 | 1.66 | 1.28 | 1.18 | 2.14 | 1.94 | 1.81 | 2.60 | 0.57 |
| Th | 0.68 | 0.58 | 2.86 | 4.18 | 4.71 | 5.26 | 3.62 | 4.30 | 5.42 | 6.00 | 5.59 | 4.54 | 1.91 |
| U | 0.15 | 0.15 | 0.64 | 0.94 | 0.95 | 1.18 | 0.89 | 0.93 | 1.27 | 1.30 | 1.31 | 0.96 | 0.47 |

Notes: Total iron reported as $FeO^{total}$, oxides in wt %, trace elements in ppm, LOI = loss on ignition

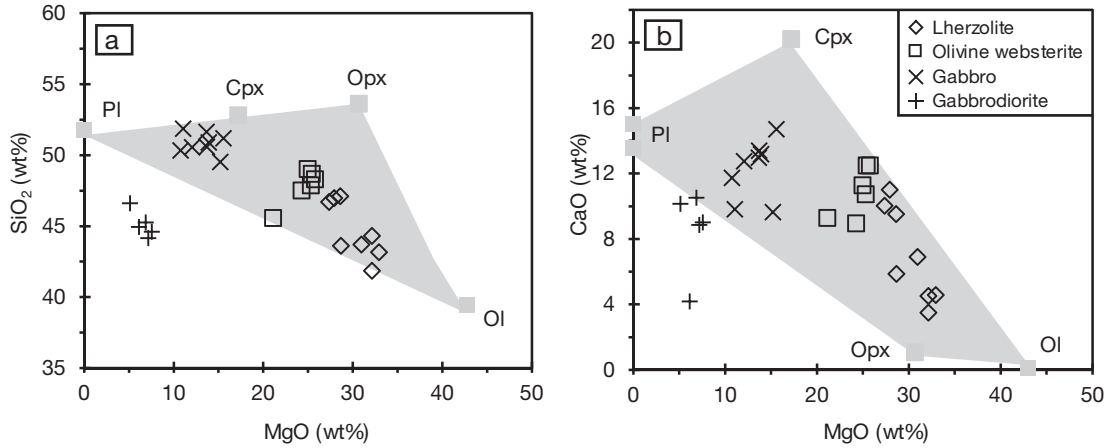


FIG. 6. Plots of $SiO_2$ (a) and CaO (b) vs. MgO in whole rocks from the Zhubu intrusion.

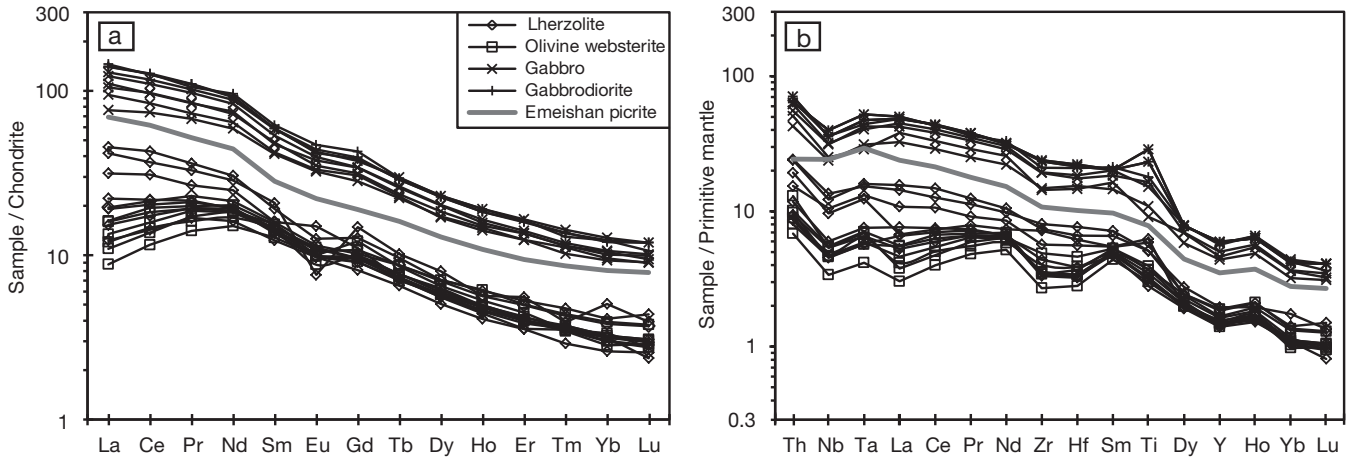


FIG. 7. Chondrite-normalized REE patterns (a) and primitive mantle-normalized alteration-resistant trace element patterns (b) of the Zhubu intrusive rocks. The average values of the Emeishan picrites are from Zhang et al. (2006). The chondrite values are from Anders and Grevesse (1989). The primitive mantle values are from Sun and McDonough (1989).

in the ultramafic and gabbroic rocks of the Zhubu intrusions are lower and higher than that of the Emeishan picrites, respectively. Some lherzolite and olivine websterite samples from the Zhubu intrusion are characterized by hump-shaped REE patterns (Fig. 7a), possibly due to the presence of abundant clinopyroxene which can fractionate light REE (Hart and Dunn, 1993; Hauri et al., 1994). Other samples from the intrusion show light REE enrichments, similar to the Emeishan picrites. Negative Nb anomalies relative to Th and Ta, which are rare in the Emeishan picrites, are common in the Zhubu intrusion (Fig. 7b). Some gabbroic rocks in the Zhubu intrusion are also characterized by positive Ti anomalies relative to Sm and Dy (Fig. 7b) due to abundant Fe-Ti oxides in these rocks.

*Chalcophile elements*

The concentrations of PGE, Cu, Ni, and S in sulfide-mineralized samples from the Zhubu intrusion are listed in Table 2. With the exception of a gabbrodiorite, all other samples from the Zhubu intrusion together show positive correlations between the chalcophile elements and S (Fig. 8). Good correlations between Pd, Pt, Ir, Ru, and Rh are also present in the samples (Fig. 9a-c). In contrast, no correlation exists between Pd and Cu in the samples (Fig. 9d).

The primitive mantle-normalized patterns of PGE and Cu in bulk sulfide (i.e., recalculated 100% sulfide or metal tenors) are illustrated in Figure 10. To reduce the uncertainties associated with S contents in tenor calculation, only the samples with >0.1 wt % S are included in the plot. Similar to several coeval magmatic sulfide deposits in the Emeishan large igneous province, the Zhubu deposit are characterized by minor PPGE (Pt and Pd) enrichments relative to IPGE (Ir, Ru ,and Rh). The metal tenors of bulk sulfides in the layered sequence of the Zhubu intrusion are as low as in the Limahe Ni-Cu deposit. The metal tenors of bulk sulfides in the margin of the Zhubu intrusion are significantly higher, up to the values in the Jinbaoshan Pt-Pd deposit.

*Rb-Sr and Sm-Nd isotopes*

The Rb-Sr and Sm-Nd isotopes of the Zhubu intrusion are listed in Table 3. The initial isotopic ratios were calculated using the crystallization age of 261 Ma which was determined by SHRIMP zircon dating (Zhou et al., 2008). The $(^{87}Sr/^{86}Sr)_i$ ratios of the Zhubu intrusion range from 0.709591 to 0.710692. The $\varepsilon_{Nd}$ values of the intrusion vary between –2.3 and –3.1. A comparison with several coeval sulfide ore-bearing intrusions and the Emeishan flood basalts is shown in Figure 11. The Zhubu intrusion is characterized by higher $(^{87}Sr/^{86}Sr)_i$ ratios and lower $\varepsilon_{Nd}$ values than the other sulfide ore-bearing intrusions in the Emeishan large igneous province. The $\varepsilon_{Nd}$ values of the Zhubu intrusion are similar to that of some of the coeval basalts. However, the $(^{87}Sr/^{86}Sr)_i$ ratios of the Zhubu intrusion are significantly higher.

## Modeling and Discussion

*Parental magma composition*

Cr spinel compositions indicate that the Zhubu magma was more fractionated than the liquid composition of the Emeishan picrites when Cr-spinel appeared on the liquidus. Clinopyroxene data (Fig. 5) indicate that the Zhubu magma had higher Cr and lower Ti contents than the magma of the Emeishan picrites by the time clinopyroxene appeared on the liquidus. The most primitive clinopyroxene phenocrysts in the Emeishan picrites have Mg numbers similar to clinopyroxene in the Zhubu ultramafic rocks (Fig. 5), indicating that the composition of the Zhubu magma was similar to the liquid composition of the Emeishan picrites when clinopyroxene started to crystallize from the liquid.

Table 2. Chalcophile Element Concentrations in the Zhubu Intrusive Rocks

| Sample no. | Rock type | S | Ni | Cu | Ir | Ru | Rh | Pt | Pd |
|---|---|---|---|---|---|---|---|---|---|
| ZB07 | Lherzolite | 0.14 | 1,139 | 65.4 | 1.47 | 1.33 | 0.51 | 21.48 | 7.77 |
| ZB08 | Lherzolite | 0.09 | 989 | 35.4 | 3.02 | 3.44 | 0.81 | 33.72 | 11.17 |
| ZB10 | Lherzolite | 0.11 | 969 | 127.2 | 0.46 | 0.29 | 0.17 | 11.92 | 4.39 |
| ZB11 | Lherzolite | 0.10 | 954 | 186.4 | 0.47 | 0.31 | 0.15 | 11.53 | 4.60 |
| ZB14 | Lherzolite | 0.08 | 1,186 | 482.6 | 0.36 | 0.26 | 0.12 | 8.36 | 35.31 |
| ZB25 | Lherzolite | 0.08 | 1,254 | 26.0 | 1.01 | 1.42 | 0.37 | 17.85 | 7.04 |
| P4-2 | Lherzolite | 0.32 | 1,738 | 775.0 | 23.9 | 12.0 | 11.9 | 658.0 | 376.0 |
| Z5 | Lherzolite | 0.18 | 1,254 | 219.0 | 1.68 | 4.37 | 0.57 | 17.60 | 7.06 |
| ZB05 | Olivine websterite | 0.17 | 3,054 | 856.4 | 9.14 | 3.71 | 2.95 | 528.1 | 103.9 |
| ZB06 | Olivine websterite | 0.16 | 811 | 363.5 | 0.34 | 0.16 | 0.07 | 5.68 | 2.73 |
| ZB12 | Olivine websterite | 0.12 | 880 | 168.1 | 0.34 | 0.25 | 0.10 | 8.17 | 2.90 |
| ZB13 | Olivine websterite | 0.13 | 967 | 286.2 | 0.55 | 0.44 | 0.16 | 9.72 | 4.48 |
| ZB15 | Olivine websterite | 0.14 | 846 | 175.5 | 0.39 | 0.71 | 0.07 | 3.43 | 2.53 |
| KT31-15 | Olivine websterite | 0.17 | 939 | 154.0 | 0.39 | 0.71 | 0.07 | 3.43 | 2.53 |
| ZB17 | Gabbro | 0.07 | 314 | 212.1 | 0.16 | 0.53 | 0.07 | 0.56 | 0.63 |
| ZB18 | Gabbro | 0.03 | 212 | 163.1 | 0.04 | 0.04 | 0.01 | 0.12 | 0.24 |
| ZB19 | Gabbro | 0.03 | 148 | 107.1 | 0.05 | 0.04 | 0.01 | 0.06 | 0.29 |
| ZB20 | Gabbro | 0.03 | 122 | 100.4 | 0.04 | 0.02 | 0.02 | 0.23 | 0.47 |
| P4U2 | Gabbro | 0.13 | 323 | 76.9 | 0.24 | 0.45 | 0.05 | 0.92 | 2.19 |
| ZB23 | Gabbrodiorite | 0.06 | 35 | 59.3 | 0.02 | 0.03 | 0.00 | 0.06 | 0.24 |
| ZB24 | Gabbrodiorite | 0.03 | 24 | 69.0 | 0.02 | 0.02 | 0.00 | 0.04 | 0.12 |
| P4-1 | Gabbrodiorite | 0.34 | 18 | 29.8 | 0.08 | 0.34 | 0.03 | 0.47 | 1.21 |
| P4U1 | Gabbrodiorite | 0.38 | 1,857 | 695 | 37.8 | 16.3 | 17.8 | 970 | 505 |

Notes: S in wt %, Ni and Cu in ppm, PGE in ppb

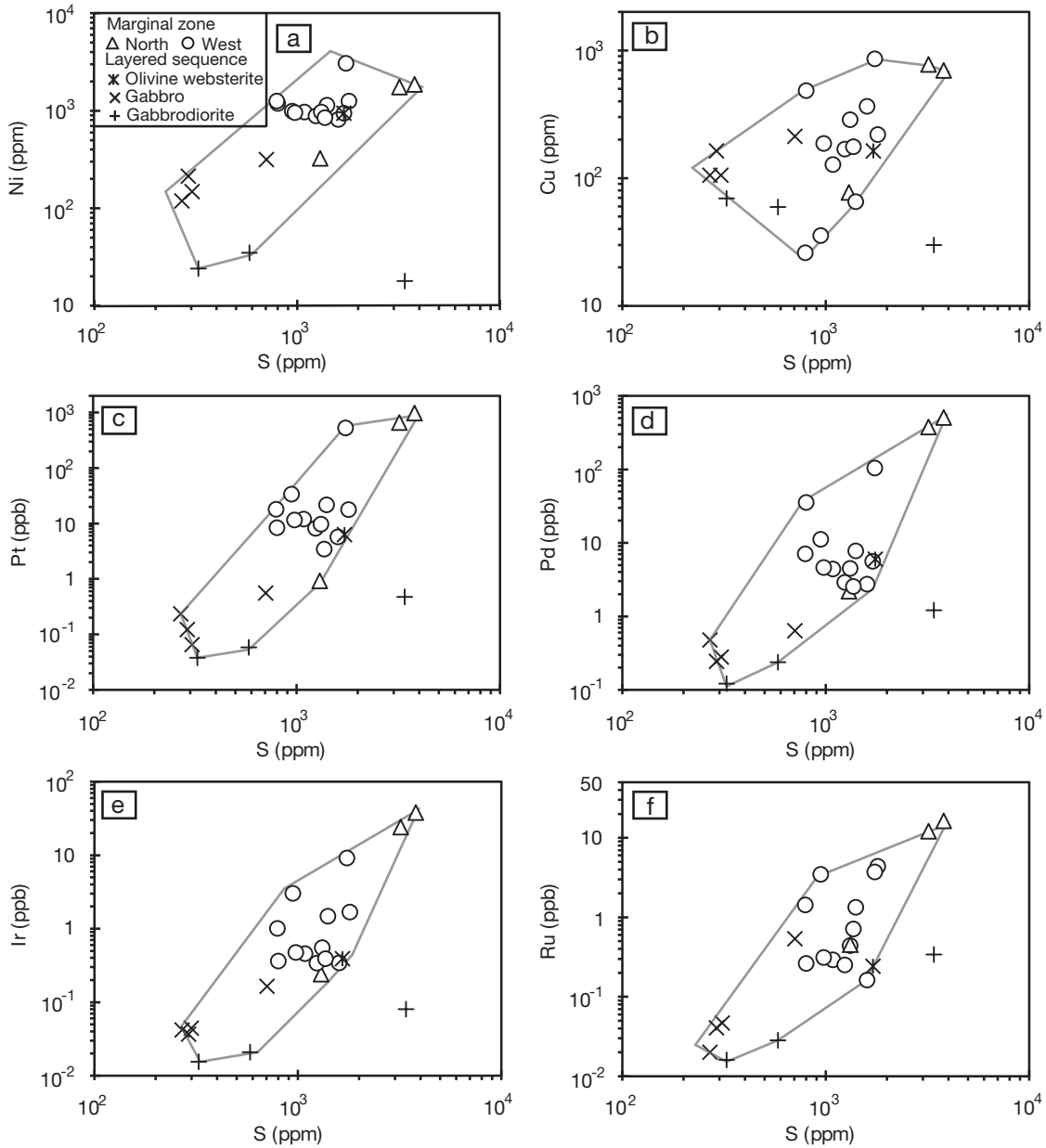


FIG. 8. Plots of chalcophile elements vs. S in whole rocks from the Zhubu intrusion.

Olivine Fo content is a function of MgO/FeO in magma (Roeder and Emslie, 1970). The Fo contents of olivine in the Zhubu ultramafic rocks are similar to the rim composition of zoned olivine phenocrysts in the Emeishan picrites (Li et al., 2012). These authors suggested that the rims of zoned olivine phenocrysts in the Emeishan picrites crystallized from the transporting magma prior to eruption. A comparison of olivine Fo contents between the Zhubu intrusion and the Emeishan picrites reveals that the parental magma of the Zhubu intrusion and the transporting magma of the Emeishan picrites have similar MgO/FeO ratios.

Good correlations between PGE and S (Fig. 8) and between individual PGE in whole rocks (Fig. 9) indicate that the chalcophile elements in the Zhubu intrusion are mainly controlled by magmatic sulfides. We have used the mass-balance equation of Campbell and Naldrett (1979) and a partition coefficient of $10^5$ for all PGE between sulfide liquid and magma, which is within the range of experimental results (see summary in Naldrett, 2011), to estimate the initial concentrations of PGE in the Zhubu magma and the R factors (magma/sulfide, mass ratio) for the Zhubu deposit. The results are shown in Figure 12. The estimated R factors vary from ~100 to ~6,000. The estimated initial magma compositions are 7 ppb Pd, 9.3 ppb Pt, and 0.8 ppb Ir. These values are similar to that of the Emeishan picrites (Wang et al., 2007; Li et al., 2012).

*Crustal contamination and sulfide saturation*

Negative Nb anomalies relative to Th and Ta in the Zhubu intrusion (Fig. 7b) indicate that its parental magma was contaminated by crustal materials. As shown in Figure 11, the

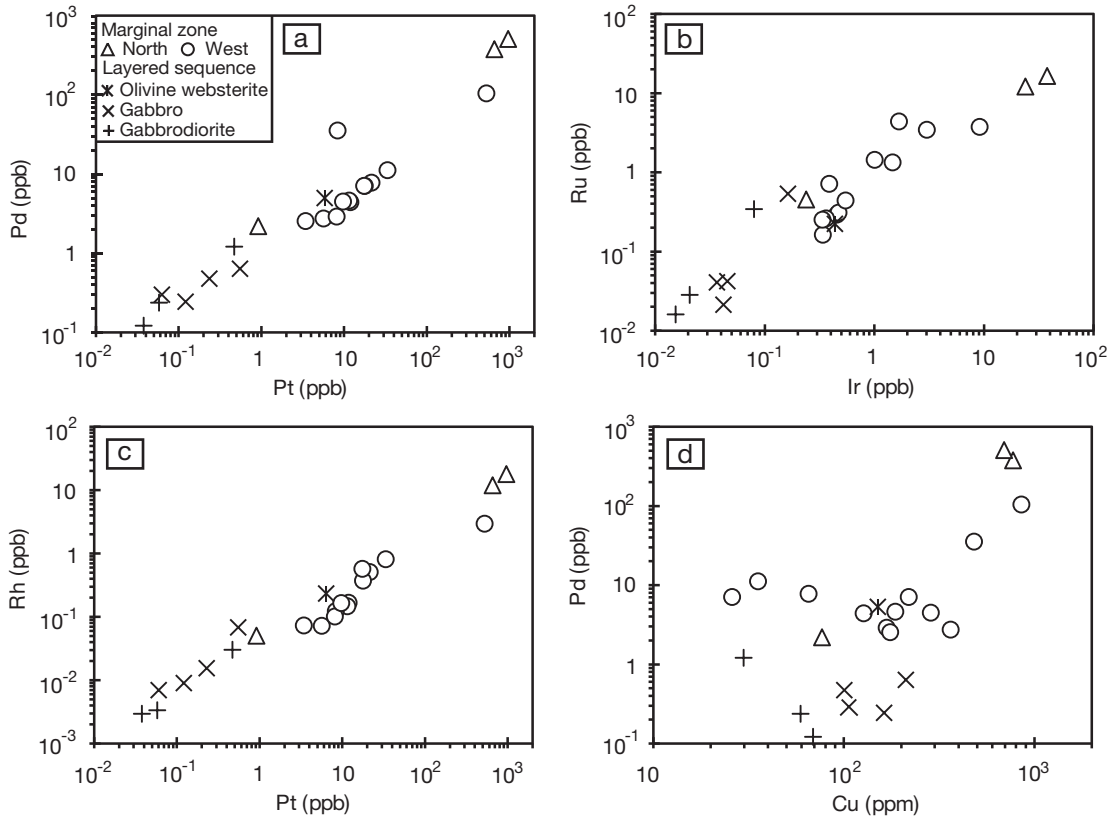


FIG. 9. Relationships between some chalcophile elements in whole rocks from the Zhubu intrusion.

Sr-Nd isotope compositions of the Zhubu intrusion are consistent with 25 to 35 wt % bulk assimilation of the upper crust by a mantle-derived magma with isotopic compositions similar to the uncontaminated picrites in the region. The amounts of crustal materials required to explain the Zhubu isotope data would be lower if selective assimilation instead of bulk assimilation was involved. The trace element and Sr-Nd isotope signatures are consistent with the interpretation that sulfide saturation in the Zhubu magma was triggered by crustal contamination. Whether or not crustal sulfur was also involved is an important question to be addressed when S-Os isotopes become available.

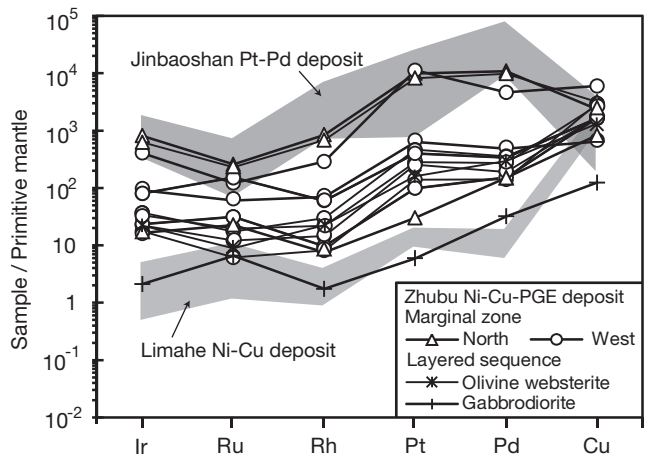


FIG. 10. Primitive mantle-normalized PGE patterns of sulfide-bearing samples from the Zhubu intrusion. The normalization values are from Barnes and Maier (1999).

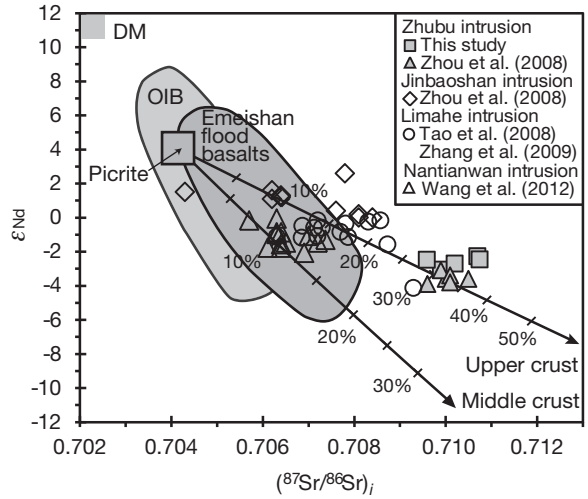


FIG. 11. Plot of $\varepsilon_{Nd}$ ($t$ = 260 Ma) vs. $(^{87}Sr/^{86}Sr)_i$ for the Zhubu intrusion. Data for oceanic island basalts (OIB) and depleted mantle (DM) are from Sun and McDonough (1989) and Zindler and Hart (1986), respectively. Values used in the mixing calculations: Emeishan picrite, 130 ppm Sr, 10.5 ppm Nd, $(^{87}Sr/^{86}Sr)_i$, 0.70418, $\varepsilon_{Nd}$, 4; middle crust, 282 ppm Sr, 25 ppm Nd, $(^{87}Sr/^{86}Sr)_i$, 0.715, $\varepsilon_{Nd}$, −22; upper crust, 320 ppm Sr, 27 ppm Nd, $(^{87}Sr/^{86}Sr)_i$, 0.715, $\varepsilon_{Nd}$, −10. The Emeishan picrite data are from Zhang et al. (2006). The concentrations of Sr and Nd in the crusts are from Rudnick and Gao (2003). The Sr and Nd isotopes in the crusts are from Chen and Jahn (1998).

TABLE 3. Whole-Rock Sr-Nd Isotope Compositions, Zhubu Mafic-Ultramafic Intrusion

| Sample no. | Rock type | Rb | Sr | Sm | Nd | $^{87}Rb/^{86}Sr$ | $^{87}Sr/^{86}Sr$ | $2\sigma$ | $^{147}Sm/^{144}Nd$ | $^{143}Nd/^{144}Nd$ | $2\sigma$ | $(^{87}Sr/^{86}Sr)_i$ | $\varepsilon_{Nd}$ |
|---|---|---|---|---|---|---|---|---|---|---|---|---|---|
| Z5 | Lherzolite | 30.83 | 374.10 | 3.60 | 20.05 | 0.2371 | 0.710776 | 0.00001 | 0.1087 | 0.512331 | 0.000015 | 0.709899 | –3.06 |
| P4U2 | Gabbro | 30.05 | 268.40 | 8.61 | 35.25 | 0.3224 | 0.711394 | 0.000011 | 0.1479 | 0.512416 | 0.000011 | 0.710201 | –2.71 |
| V3-6 | Gabbro | 16.17 | 312.00 | 7.94 | 36.03 | 0.1493 | 0.711244 | 0.000011 | 0.1334 | 0.512414 | 0.000011 | 0.710692 | –2.27 |
| V2 | Gabbrodiorite | 57.46 | 673.90 | 9.35 | 44.38 | 0.2455 | 0.710499 | 0.00001 | 0.1275 | 0.512393 | 0.000011 | 0.709591 | –2.47 |
| P4-1 | Gabbrodiorite | 32.09 | 135.50 | 9.23 | 43.71 | 0.6824 | 0.713265 | 0.000012 | 0.1279 | 0.512394 | 0.000011 | 0.710741 | –2.46 |

Notes: $\varepsilon_{Nd}$ is the derivation in parts per 10,000 of the initial ratio from that of a chondritic reservoir at the crystallization age of 261 Ma

*A genetic model and exploration implications*

As shown in Figure 4, olivine in the Zhubu intrusion is depleted in Ni as compared to olivine phenocrysts in the Emeishan picrites. This, together with the occurrence of small sulfide inclusions in olivine crystals in the intrusion, indicates that sulfide segregation started before olivine crystallization at Zhubu. The petrological and geochemical characteristics described above are consistent with a two-stage genetic model for the Zhubu intrusion: an early conduit stage and a late in situ differentiation stage. In this model the marginal zone and the layered sequence are believed to have formed at the early and late stages, respectively. Sulfide segregation is thought to have occurred at the conduit stage. Highly variable metal tenors of bulk sulfides in the marginal zone indicate variable reaction of immiscible sulfide liquids with new magma passing through the conduit.

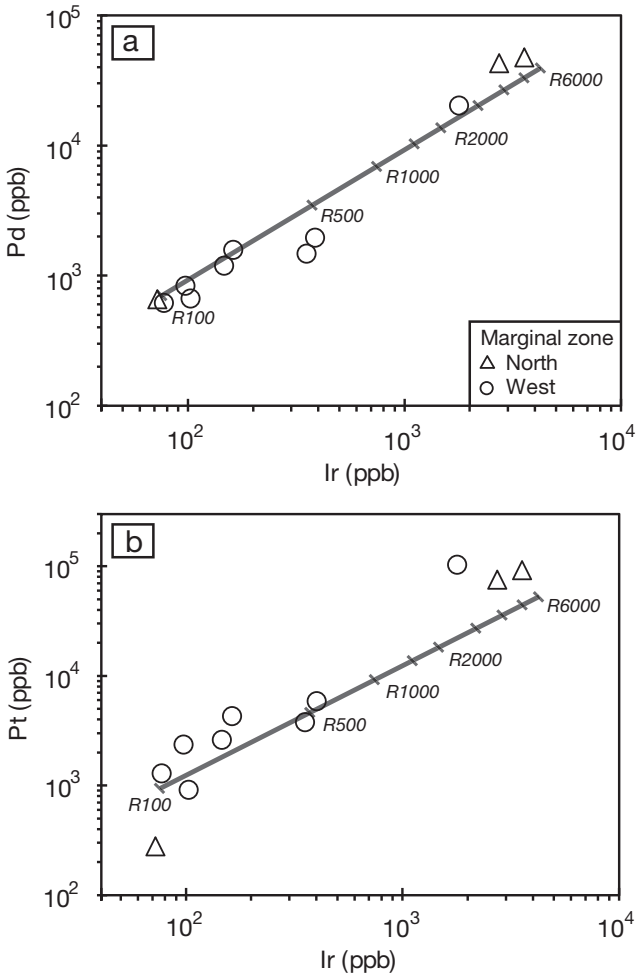


FIG. 12. Modeling of PGE variations in sulfide liquids segregated from magma with variable R factors (magma/sulfide, mass ratio) for the Zhubu deposit using the mass-balance equation of Campbell and Naldrett (1979) and a partition coefficient of $10^5$ for the PGE between sulfide liquid and magma. The results show that the compositions of bulk sulfides (recalculated to 100% sulfides) in the Zhubu deposit can be explained by variable R factors from 100 to 6,000 and initial magma containing 7 ppb Pd, 9.3 ppb Pt and 0.8 ppb Ir.

The metal tenors of the Zhubu deposit are as high as other important magmatic Ni-Cu-PGE sulfide deposits in the Emeishan large igneous province. However, the grades of the Zhubu deposit are rather low, which makes it less attractive to mine under current market conditions. High-grade sulfide mineralization may exist in the lower part of the conduit of the Zhubu magmatic system. Based on the lesson from the Voisey's Bay deposit (Li and Naldrett, 1999; Lightfoot and Naldrett, 1999), we suggest that future exploration at Zhubu focus in the area where most significant uplifting by faulting may have occurred.

## Conclusions

Several important conclusions can be made from this study. They are summarized below.

1. Olivine data indicate that the parental magma of the Zhubu ultramafic intrusive rocks and the transporting magma of the Emeishan picrites have similar MgO/FeO ratios.
2. Depletion of Ni in olivine from the Zhubu intrusion indicates that sulfide segregation took place before olivine crystallization.
3. The initial concentrations of PGE in the Zhubu magma were high and similar to the values in the Emeishan picrites.
4. Whole-rock trace element and Sr-Nd isotope data are consistent with the interpretation that sulfide saturation in the Zhubu magma was triggered by crustal contamination.
5. The Zhubu intrusion can be explained by two stages of formation: a conduit stage for the sulfide ore-bearing marginal zone and an in situ differentiation stage for the layered sequence.
6. The area where the lower part of the conduit may have been brought up by faulting should be the focus of future exploration at Zhubu.

## Acknowledgments

This work was financially supported by the National Science Foundation of China (grants 41072056 and 40973039),

the State Key Laboratory of Ore Deposit Geochemistry of China (grants 201110 and 201205) and Scholarship Award for Excellent Doctoral Student granted by Lanzhou University. Thoughtful comments from two anonymous reviewers and useful editorial inputs from Peter Lightfoot are appreciated. Xie-Yan Song, Lie-Meng Chen, Piaoer Fu, and Maochao Zhang are thanked for assistance in sampling and PGE analysis. The revision was carried out during Qingyan Tang's visit to Indiana University, which was financially supported by China Scholarship Council (201206180107).

## REFERENCES

Anders, E., and Grevesse, N., 1989, Abundances of the elements: Meteoritic and solar: Geochimica et Cosmochimica Acta, v. 53, p. 197–214.

Arndt, N.T., 2011, Insights into the geologic settings and origin of Ni-Cu-PGE sulfide deposits of the Noril'sk-Talnakh region, Siberia: Reviews in Economic Geology, v. 17, p. 199–215.

Barnes, S.-J., and Maier, W.D., 1999, The fractionation of Ni, Cu, and the noble metals in silicate and sulfide liquids: Geological Association of Canada Short Course Notes, v. 13, p. 69–106.

Campbell, I.H., and Naldrett, A.J., 1979, The influence of silicate:sulfide ratios on the geochemistry of magmatic sulfides: Economic Geology, v. 74, p. 1503–1506.

Chen, J., and Jahn, B.-M., 1998, Crustal evolution of southeastern China: Nd and Sr isotopic evidence: Tectonophysics, v. 284, p. 101–133.

Chung, S.-L., and Jahn, B.-M., 1995, Plume-lithosphere interaction ingeneration of the Emeishan flood basalts at the Permian-Triassic boundary: Geology, v. 23, p. 889–892.

Fan, W., Zhang, C., Wang, Y., Guo, F., and Peng, T., 2008, Geochronology and geochemistry of Permian basalts in western Guangxi Province, southwest China: Evidence for plume-lithosphere interaction: Lithos, v. 102, p. 218–236.

Hart, S.R., and Dunn, T., 1993, Experimental cpx/melt partitioning of 24 trace elements: Contributions to Mineralogy and Petrology, v. 113, p. 1–8.

Hauri, E.H., Wagner, T.P., and Grove, T.L., 1994, Experimental and natural partitioning of Th, U, Pb and other trace elements between garnet, clinopyroxene and basaltic melts: Chemical Geology, v. 117, p. 149–166.

Kamo, S.L., Czamanske, G.K., Amelin, Y., Fedorenko, V.A., Davis, D.W., and Trofimov, V.R., 2003, Rapid eruption of Siberian flood volcanic rocks and evidence for coincidence with the Permian-Triassic boundary and mass extinction at 251 Ma: Earth and Planetary Science Letters, v. 214, p. 75–91.

Li, C., and Naldrett, A.J., 1999, The geology and petrology of the Voisey's Bay intrusion: Reaction of olivine with trapped sulfide and silicate liquids: Lithos, v. 47, p. 1–31.

Li, C., Maier, W.D., and de Waal, S.A., 2001, Magmatic Ni-Cu versus PGE deposits: Contrasting genetic controls and exploration implication: South African Journal of Geology, v. 104, p. 309–318.

Li, C., Ripley, E.M., Tao, Y., and Mathez, E.A., 2008, Cr-spinel/olivine and Cr-spinel/liquid nickel partition coefficients from natural samples: Geochimica et Cosmochimica Acta, v. 72, p. 1678–1684.

Li, C., Ripley, E.M., and Naldrett, A.J., 2009, A new genetic model for the giant Ni-Cu-PGE sulfide deposits associated with the Siberian flood basalts: Economic Geology, v. 104, p. 291–301.

Li, C., Tao, Y., Qi, L., and Ripley, E.M., 2012, Controls on PGE fractionation in the Emeishan picrites and basalts: Constraints from integrated lithophile-siderophile elements and Sr-Nd isotopes: Geochimica et Cosmochimica Acta, v. 90, p. 12–32.

Lightfoot, P.C., and Keays, R.R., 2005, Siderophile and chalcophile metal variations in flood basalts from the Siberian trap, Noril'sk region: Implications for the origin of the Ni-Cu-PGE sulfide ores: Economic Geology, v. 100, p. 439–462.

Lightfoot, P.C., and Naldrett, A.J., 1999, Geological and geochemical relationships in the Voisey's Bay intrusion, Nain Plutonic Suite, Labrador, Canada: Geological Association of Canada Short Course Notes, v. 13, p. 1–30.

Naldrett, A.J., 2011, Fundamentals of magmatic sulfide deposits: Reviews in Economic Geology, v. 17, p. 1–50.

Qi, L., and Zhou M.-F., 2008, Platinum-group elemental and Sr-Nd-Os isotopic geochemistry of Permian Emeishan flood basalts in Guizhou Province, SW China: Chemical Geology, v. 248, p. 83–103.

Qi, L., Gao, J., Huang, X., Hu, J., Zhou, M.-F., and Zhong, H., 2011, An improved digestion technique for determination of platinum group elements in geological samples: Journal of Analytical Atomic Spectrometry, v. 26, p. 1900–1904.

Roeder, P.L., and Emslie, R.F., 1970, Olivine-liquid equilibrium: Contributions to Mineralogy and Petrology, v. 29, p. 275–289.

Rudnick, R.L., and Gao, S., 2003. Composition of the continental crust: Treatise on Geochemistry, v. 3, p. 1–64.

Song, X.-Y., Zhou, M.-F, Hou, Z.-Q., Cao, Z.-M., Wang, Y.-L., and Li, Y., 2001, Geochemical constraints on the mantle source of the upper Permian Emeishan continental flood basalts, southern China: International Geology Review, v. 43, p. 213–225.

Song, X.-Y., Zhou, M.-F., Cao, Z.M., Sun, M., and Wang, Y., 2003, Ni-Cu-(PGE) magmatic sulfide deposits in the Yangliuping area, Permian Emeishan igneous province, SW China: Mineralium Deposita, v. 38, p. 831–843.

Song, X.-Y., Keays, R.R., Xiao, L., Qi, H.-W., and Ihlenfeld, C., 2009, Platinum-group element geochemistry of the continental flood basalts in the central Emeisihan large igneous province, SW China: Chemical Geology, v. 262, p. 246–261.

Sun, S.-S., and McDonough, W.F., 1989, Chemical and isotopic systematics in ocean basalt: Implication for mantle composition and processes: Geological Society of London Special Publication 42, p. 313–345.

Tao, Y., Li, C., Hu, R., Ripley, E.M., Du, A., and Zhong, H., 2007, Petrogenesis of the Pt-Pd mineralized Jinbaoshan ultramafic intrusion in the Permian Emeishan large igneous province, SW China: Contributions to Mineralogy and Petrology, v. 153, p. 321–337.

Tao, Y., Li, C., Song, X.-Y., and Ripley, E.M., 2008, Mineralogical, petrological, and geochemical studies of the Limahe mafic-ultramatic intrusion and associated Ni-Cu sulfide ores, SW China: Mineralium Deposita, v. 43, p. 849–872.

Tao, Y., Li, C., Hu, R., Qi, L., Qu, W., and Du, A., 2010, Re-Os isotopic constraints on the genesis of the Limahe Ni-Cu deposit in the Emeishan large igneous province, SW China: Lithos, v. 119, p. 137–14.

TGT-YBGR (Third Geological Team, Yunnan Bureaus of Geology and Resources), 1970, Reserves report of Zhubu Pt deposit in Yuanmou of Yunnan Province: Internal Report, 170 p. (in Chinese).

Wang, C.Y., Zhou, M.F., and Zhao, D., 2005, Mineral chemistry of chromite from the Permian Jinbaoshan Pt-Pd-sulphide-bearing ultramafic intrusion in SW China, with petrogenetic implications: Lithos, v. 83, p. 47–66.

Wang, C.Y., Zhou, M.F., and Keays, R.R., 2006, Geochemical constraints on the origin of the Permian Baimazhai maficultramafic intrusion, SW China: Contributions to Mineralogy and Petrology, v. 152, p. 309–321.

Wang, C.Y., Zhou, M.-F., and Qi. L., 2007, Permian basalts and mafic intrusions in the Jinping (SW China)-Song Da (northern Vietnam) district: Mantle sources, crustal contamination and sulfide segregation: Chemical Geology, v. 243, p. 317–343.

——2011, Chalcophile element geochemistry and petrogenesis of high-Ti and low-Ti magmas in the Permian Emeishan large igneous province, SW China: Contributions to Mineralogy and Petrology, v. 161, p. 237–254.

Wang, C.Y., Zhou M.-F., Sun, Y., and Arndt, N.T., 2012, Differentiation, crustal contamination and emplacement of magmas in the formation of the Nantianwan mafic intrusion of the ~260 Ma Emeishan large igneous province, SW China: Contributions to Mineralogy and Petrology, v. 164, p. 281–301.

Zhang, Z., Mahoney, J.J., Mao, J., and Wang, F., 2006, Geochemistry of picritic and associated basalt flows of the western Emeishan flood basalt province: Journal of Petrology, v. 47, p. 1997–2019.

Zhou, M.-F., Arndt, N.T., Malpas, J., Wang, C.Y., and Kennedy, A., 2008, Two magma series and associated ore deposit types in the Permian Emeishan large igneous province, SW China: Lithos, v. 103, p. 352–368.

Zindler, A., and Hart, S.R., 1986, Chemical geodynamics: Annual Review of Earth and Planetary Sciences, v. 14, p. 493–571.

TABLE A1. Chemical Compositions of Minerals, Zhubu Mafic-Ultramafic Intrusion

Olivine

| Sample | Rock type | *n* | $SiO_2$ | FeO | MnO | MgO | CaO | NiO | Total | Fo | Ni |
|---|---|---|---|---|---|---|---|---|---|---|---|
| ZB07 | Lherzolite | 7 | 38.39 | 17.66 | 0.24 | 42.88 | 0.12 | 0.22 | 99.50 | 81.2 | 1,768 |
| ZB08 | Lherzolite | 9 | 38.77 | 17.30 | 0.26 | 43.16 | 0.14 | 0.22 | 99.85 | 81.6 | 1,716 |
| ZB10 | Lherzolite | 29 | 38.85 | 16.16 | 0.23 | 44.30 | 0.12 | 0.24 | 99.90 | 82.9 | 1,891 |
| ZB11 | Lherzolite | 8 | 39.00 | 15.56 | 0.23 | 44.71 | 0.15 | 0.24 | 99.90 | 83.6 | 1,889 |
| ZB14 | Lherzolite | 10 | 39.32 | 15.81 | 0.24 | 44.28 | 0.14 | 0.24 | 100.02 | 83.3 | 1,860 |
| ZB25 | Lherzolite | 20 | 39.15 | 16.88 | 0.24 | 43.73 | 0.16 | 0.23 | 100.38 | 82.2 | 1,814 |
| ZB12 | Olivine websterite | 9 | 39.35 | 16.33 | 0.22 | 44.34 | 0.12 | 0.23 | 100.59 | 82.8 | 1,774 |
| ZB13 | Olivine websterite | 6 | 38.93 | 17.48 | 0.24 | 43.04 | 0.11 | 0.24 | 100.05 | 81.4 | 1,873 |
| ZB15 | Olivine websterite | 9 | 39.08 | 16.68 | 0.25 | 44.03 | 0.12 | 0.21 | 100.37 | 82.4 | 1,655 |

Clinopyroxene

| Sample | Rock type | *n* | $SiO_2$ | $TiO_2$ | $Al_2O_3$ | FeO | MnO | MgO | CaO | $Cr_2O_3$ | Total | Mg# |
|---|---|---|---|---|---|---|---|---|---|---|---|---|
| ZB07 | Lherzolite | 2 | 52.49 | 0.77 | 2.13 | 5.52 | 0.09 | 16.92 | 21.06 | 0.97 | 99.95 | 84.54 |
| ZB11 | Lherzolite | 10 | 52.55 | 0.66 | 1.61 | 4.95 | 0.10 | 17.46 | 21.30 | 0.79 | 99.42 | 86.27 |
| ZB14 | Lherzolite | 7 | 52.92 | 0.43 | 1.65 | 5.00 | 0.10 | 17.00 | 21.13 | 0.86 | 99.09 | 85.85 |
| ZB06 | Olivine websterite | 9 | 53.25 | 0.33 | 1.58 | 5.20 | 0.12 | 16.97 | 21.22 | 0.71 | 99.38 | 85.31 |
| ZB12 | Olivine websterite | 3 | 52.64 | 0.57 | 1.90 | 5.06 | 0.11 | 16.91 | 21.02 | 0.94 | 99.16 | 85.61 |
| ZB15 | Olivine websterite | 2 | 52.19 | 0.60 | 1.72 | 4.90 | 0.09 | 16.52 | 21.12 | 0.87 | 98.01 | 85.73 |

Cr spinel inclusions within olivine crystals

| Sample | Rock type | *n* | $TiO_2$ | $Al_2O_3$ | FeO | MnO | MgO | $Cr_2O_3$ | NiO | Total | Cr# |
|---|---|---|---|---|---|---|---|---|---|---|---|
| ZB11 | Lherzolite | 6 | 3.15 | 8.00 | 47.01 | 0.04 | 3.78 | 36.26 | 0.19 | 100.32 | 75.16 |

Notes: *n* = number of analysis; oxide in wt %, Fo in mol %; Ni in ppm, Cr# = 100 × Cr/(Cr + Al), molar; Mg# = 100 × Mg/(Mg+$Fe^{total}$), molar